Evolution from Unconventional Spin Density Wave to Superconductivity and a Pseudogaplike Phase in $NaFe_{1-x}Co_xAs$

Xiaodong Zhou,[1] Peng Cai,[1] Aifeng Wang,[2] Wei Ruan,[1] Cun Ye,[1] Xianhui Chen,[2] Yizhuang You,[3] Zheng-Yu Weng,[3] and Yayu Wang[1,*]

[1]*State Key Laboratory of Low Dimensional Quantum Physics, Department of Physics, Tsinghua University, Beijing 100084, People's Republic of China*

[2]*Hefei National Laboratory for Physical Science at Microscale and Department of Physics, University of Science and Technology of China, Hefei, Anhui 230026, People's Republic of China*

[3]*Institute for Advanced Study, Tsinghua University, Beijing 100084, People's Republic of China*

(Received 6 May 2012; published 17 July 2012)

We report the doping, temperature, and spatial evolutions of the electronic structure of $NaFe_{1-x}Co_xAs$ studied by scanning tunneling microscopy. In the parent state we directly observe the spin density wave gap, which exhibits unconventional features that are incompatible with simple Fermi surface nesting. The optimally doped sample has a single superconducting gap, but in the overdoped regime a novel pseudogaplike feature emerges. The pseudogaplike phase coexists with superconductivity in the ground state, persists well into the normal state, and shows strong spatial variations. The characteristics of the three distinct electronic states revealed here shed important new lights on the microscopic models for the iron-based superconductors.

DOI: 10.1103/PhysRevLett.109.037002 PACS numbers: 74.70.Xa, 74.25.Dw, 74.25.Jb, 74.55.+v

Similar to the cuprates and heavy fermion compounds, the iron pnictides represent a new family of unconventional superconductors with the superconducting (SC) phase lying in close proximity to a magnetically ordered phase [1,2]. A central debate concerning the pairing mechanism is the nature of the magnetism and its relationship to superconductivity. The existence of metallic conduction and well-defined Fermi surface (FS) in the parent state prompts the proposal that the magnetic ordering is a spin density wave (SDW) induced by FS nesting of itinerant electrons, and upon doping the pair scattering between the electron- and holelike FS pockets leads to superconductivity [3–6]. A drastically different viewpoint shows that the antiferromagnetic (AFM) ordering of local moments gives better description of the spin wave spectrum, and the magnetic interaction may be directly responsible for Cooper pairing in the doped case [7,8]. To reconcile the apparent conflicts, another theoretical model proposes that the local moments and itinerant electrons may coexist and the coupling between them gives rise to both the SDW and SC orders [9,10].

A key step for finding the valid theoretical model is to clarify the nature of each microscopic phase in the iron pnictides and establish a unified physical picture. Owing to its ability to probe the atomic scale electronic structure for both the occupied and empty states, scanning tunneling microscopy (STM) has played a crucial role in fulfilling this task [11]. However, up to date a comprehensive picture about the iron pnictides phase diagram is still lacking. The SDW gap in the parent state has never been directly observed despite implications from infrared spectroscopy [12]. There are also controversies regarding the coexisting or competing orders in the SC state, and whether there exists a pseudogap phase [13,14]. In this letter we present the evolution of the electronic structure of $NaFe_{1-x}Co_xAs$ studied by STM. We observe for the first time the unconventional SDW gap in the parent state and a novel pseudogaplike phase in the overdoped regime. The intricate evolution of the electronic states puts strong constraints on relevant theories for the iron pnictides.

High quality $NaFe_{1-x}Co_xAs$ single crystals are grown by the NaAs flux method as described elsewhere [15]. The STM experiments are performed with a low temperature ultrahigh vacuum system. The sample is mounted onto the sample holder at room temperature in a glove box filled with Ar gas to prevent the degradation in ambient atmosphere. After the sample mounting, the sample holder is transferred into the load-lock chamber of the STM, and the exposure to air during this step is less than 1 min. It is then transferred from the load-lock to the preparation chamber with pressure better than 10^{-10} mbar. The $NaFe_{1-x}Co_xAs$ crystal is cleaved *in situ* at $T = 77$ K and then immediately transferred into the STM stage. An electrochemically etched polycrystalline tungsten tip is used for all the measurements. Before the STM experiments on $NaFe_{1-x}Co_xAs$, the tip is treated by *in situ* *e*-beam sputtering and calibrated on a clean crystalline Au(111) surface prepared by repeated sputtering and annealing. STM topography is taken in the constant current mode, and dI/dV spectroscopy is collected using a standard lock-in technique with modulation frequency $f = 423$ Hz.

Figure 1(a) shows the schematic structure of the 111-type $NaFe_{1-x}Co_xAs$. The crystal is expected to cleave between two weakly bonded Na intercalation layers, exposing a charge neutral Na-terminated square lattice.

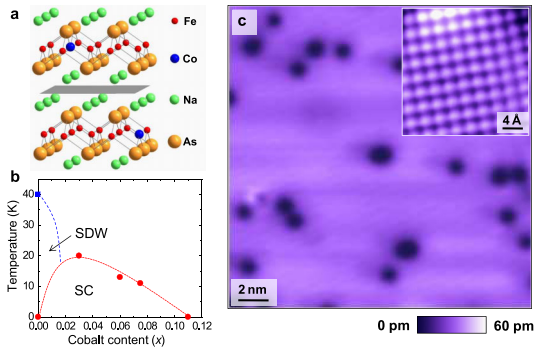

FIG. 1 (color online). (a) Schematic crystal structure of $NaFe_{1-x}Co_xAs$ where the cleavage plane is shown in grey. (b) Schematic phase diagram of $NaFe_{1-x}Co_xAs$. The red circle (blue square) marks the T_C (T_{SDW}) of the five $NaFe_{1-x}Co_xAs$ studied here. (c) Constant current image of parent NaFeAs taken with sample bias $V = -100$ mV and tunneling current $I = 50$ pA. (Inset) Close-up image taken with $V = 20$ mV and $I = 50$ pA shows a square lattice.

Figure 1(b) illustrates the electronic phase diagram of $NaFe_{1-x}Co_xAs$. With increasing Co content, the system evolves from a SDW ordered parent state to a dome-shaped SC regime and then to the non-SC metallic phase. The solid symbols mark the position of the five samples studied here, which cover each representative regime of the phase diagram. Figure 1(c) displays the topography of a parent NaFeAs surface, which is clean and flat over a large area except for the nanometer-sized dark pits (Fig. S1 [16]). The inset shows a high resolution image on a defect-free area, which reveals a square lattice with lattice constant $a \sim 4.0$ Å. This is consistent with the expected surface structure and previous STM images on similar 111 iron pnictides [17–19]. The absence of surface reconstruction and extrinsic surface states indicates that STM results on $NaFe_{1-x}Co_xAs$ may reflect the intrinsic bulk properties.

Figure 2 displays the spatially-averaged dI/dV spectroscopy, which is approximately proportional to the electron density of state (DOS). The upper panels show the dI/dV curves taken at the base temperature $T = 5$ K, and the lower panels are that taken at varied Ts. In the ground state of parent NaFeAs, we observe a well-defined energy gap around E_F [Fig. 2(a)]. With increasing T this gap is gradually filled up and closes at $T = 40$ K [Fig. 2(b)], which is the SDW transition temperature T_{SDW} determined by various techniques [20,21]. This energy gap is thus the highly anticipated SDW gap, which has never been observed before. The $T = 5$ K spectrum reveals three important features of the SDW gap. First, the gap size defined from the distance between the two peaks is $2\Delta_{SDW} = 33$ meV, which gives an anomalously large $2\Delta_{SDW}/k_BT_{SDW}$ ratio of 9.5. Second, the gap structure is

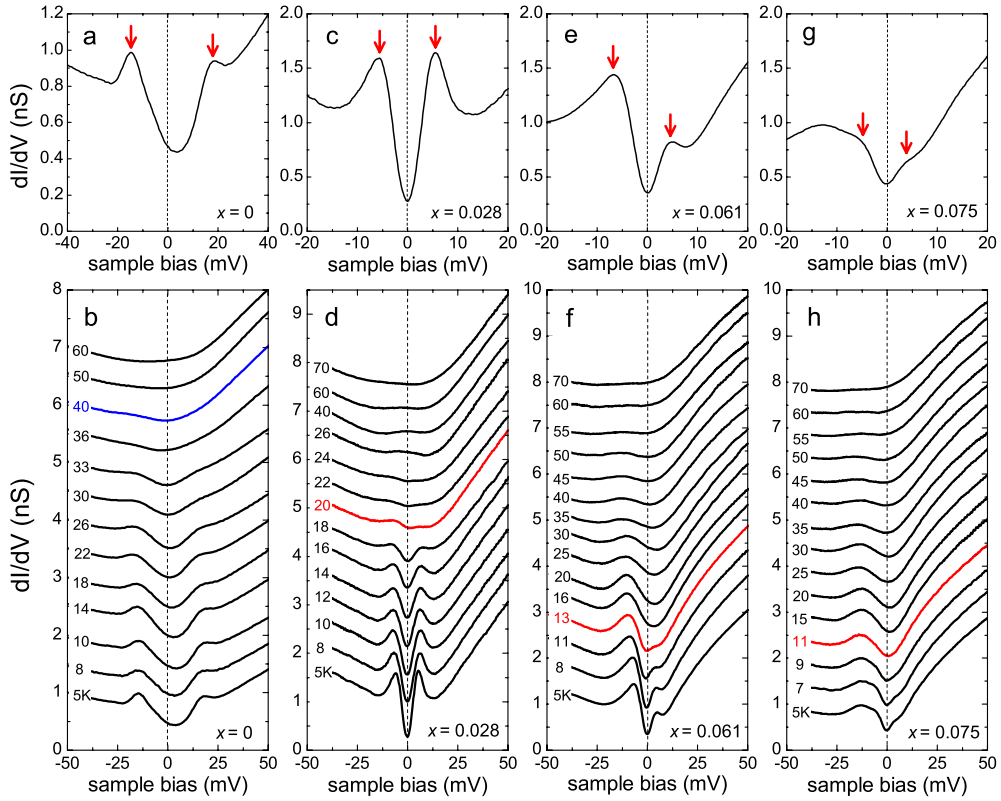

FIG. 2 (color online). Upper panels: Spatially-averaged dI/dV spectra of the $x = 0$, 0.028, 0.061 and 0.075 samples taken at $T = 5$ K. Lower panels: Temperature evolution of the dI/dV spectra of the four samples. The blue (red) curve marks the SDW (SC) transition. Vertical offset is used for clarity.

highly asymmetric with respect to E_F, apparently breaking the particle-hole symmetry. The spectrum is tilted towards positive bias with the gap bottom located at 4 meV above E_F and the two peaks located at -15 and $+18$ meV respectively. Thirdly, there is a large residual DOS at E_F even for T well below T_{SDW}, indicating that the FS is only partially gapped by the SDW order.

Figure 2(c) displays the dI/dV curve taken on the optimally doped $x = 0.028$ sample, which exhibits a sharp SC gap with well-defined coherence peaks. Unlike the SDW gap shown in Fig. 2(a), the SC gap here is highly symmetric with respect to E_F. The gap size defined from the distance between the two coherence peaks is $2\Delta_{\mathrm{SC}} = 11$ meV, giving a ratio $2\Delta_{\mathrm{SC}}/k_B T_C = 6.4$ that is close to previous STM studies on other iron pnictides [11]. The sizable residual DOS at E_F in this sample is due to the relatively high measurement temperature and disorders introduced by Co dopants [18]. Figure 2(d) shows that the SC gap closes right at $T_C = 20$ K, and in the normal state the dI/dV curves only present weak spectroscopic features.

The dI/dV curve of the overdoped $x = 0.061$ sample displays a more complex pattern. At $T = 5$ K the DOS has a minimum right at E_F, but the peak on the negative bias side has a much larger amplitude and lies further away from E_F than that on the positive side [Fig. 2(e)]. With increasing T the sharp gap feature near E_F becomes shallower and disappears above $T_C = 13$ K [Fig. 2(f)], suggesting that it is the SC gap. However, another asymmetric gaplike feature with a peak at negative bias and dip near E_F persists to the normal state and only disappears gradually at much higher T. The $x = 0.075$ sample shows a similar behavior, except that the SC gap feature [Fig. 2(g)] becomes even weaker. The SC gap in these two samples can be extracted by dividing the dI/dV curve taken at 5 K by that obtained just above T_C (Fig. S2).

To further elucidate the T evolution of the novel gaplike feature, the dI/dV curves taken at varied Ts are divided by the high T background taken at 70 K. Shown in Figs. 3(a) and 3(b) are the normalized spectra of the overdoped $x = 0.061$ and 0.075 samples. It is clear that the large, asymmetric gaplike feature coexists with the SC gap below T_C and persists well into the normal state. The T evolution is highly analogous to the pseudogap phase in underdoped cuprates [22], hence it is designated as "pseudogaplike" phase hereafter. The onset T of the pseudogaplike feature can be determined to be $T_{\mathrm{onset}} = 55$ K, when the DOS suppression near E_F first sets in.

We gain more insight into the pseudogaplike phase by taking advantage of the spatial resolution of STM. Figure 4(a) shows the topography of the $x = 0.061$ sample, which is more disordered than the parent NaFeAs due to Co doping (Fig. S3). Figure 4(b) displays the dI/dV spectra taken at $T = 5$ K along the line drawn in Fig. 4(a). In the bright area covering the majority of the surface, the dI/dV curves look similar to that shown in

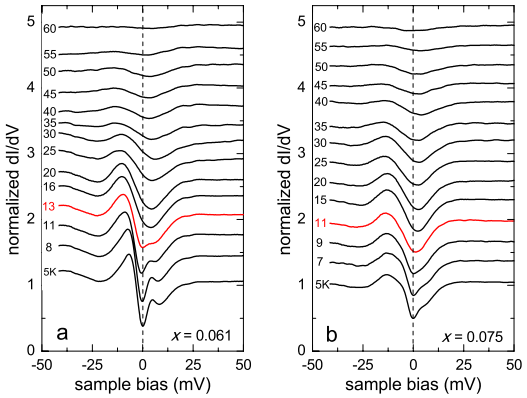

FIG. 3 (color online). The dI/dV spectra of the two overdoped $x = 0.061$ and 0.075 samples taken at varied Ts are divided by that taken at 70 K to remove the effect of high T background. The red curves mark the SC transition.

Fig. 2(e). In the minority dark area (not the dark pit), however, the energy scales of the SC gap and pseudogap become well-separated. The coexistence of the two distinct phases becomes more apparent. Figure 4(c) displays the dI/dV taken along the same line at 16 K, where the SC gap closes but the pseudogaplike feature remains and shows strong spatial variations. The normalized dI/dV spectra shown in Fig. 4(d) demonstrate that the SC gap is particle-hole symmetric and spatially uniform, in sharp contrast to the strongly asymmetric and spatially dependent pseudogaplike features in Fig. 4(c). This situation is again highly analogous to the contrasting behavior of the SC gap and pseudogap in underdoped cuprates [23,24].

The large bias dI/dV spectra of $NaFe_{1-x}Co_xAs$ reveal another unexpected trend. As shown in Fig. 5(a), the most pronounced feature here is a large "V"-shaped DOS suppression around E_F with a small residual DOS. A subtle, but highly puzzling fact is that for the four samples from $x = 0$ to 0.075, the spectra remain nearly the same. The peak at negative bias always stays at -0.2 eV and the bottom of the V-shaped suppression is pinned at E_F. We emphasize that this pinning is unrelated to the SDW or SC orders at low T (Fig. S4). This behavior is certainly incompatible with the simple band structure picture, in which a rigid band shift should be induced by electron doping. However, when x is increased further to 0.109, the high energy spectrum suddenly shifts to the left (lower energy). Meanwhile, both the SC gap and pseudogaplike features disappear all together (Fig. S5), indicating that the strongly overdoped non-SC iron pnictide behaves like a normal metal.

The rich electronic information shown above puts strong constraints on the theoretical models for the iron pnictides. The complex variations of the low energy states manifest the significant role played by the itinerant electrons, but the doping-insensitive high energy spectra indicates that the pure itinerant picture is insufficient. To resolve this dichotomy, we propose that a valid model for the iron pnictides

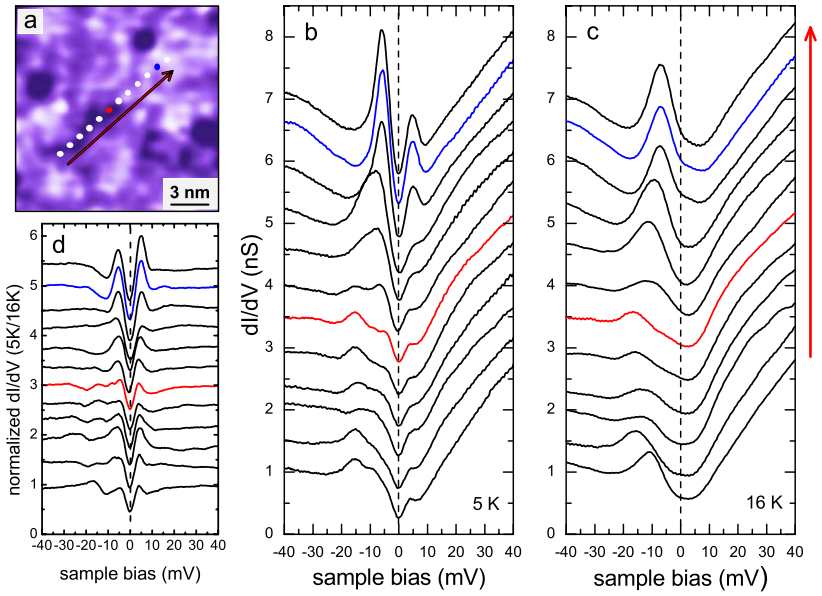

FIG. 4 (color online). (a) Topography of the $x = 0.061$ sample taken with $V = -100$ mV and $I = 100$ pA. (b) The dI/dV spectra taken at 5 K along the line in (a). Blue and red curves are two typical spectra taken at the location of the blue and red dots. (c) The spectra taken at 16 K along the same line. (d) The normalized dI/dV spectra reveal a symmetric and spatially uniform SC gap.

should involve both local moments and itinerant electrons. It was shown before that part of the five Fe d bands may be delocalized and contribute to the itinerancy, whereas the others are localized due to strong correlation effect and provide the source for local moments [25–28]. The schematic electronic structure for such a local-itinerant coexistent model is shown in Fig. 5(b) following Ref. [9]. Within this picture, the large V-shaped DOS suppression is due to a Mott-like gap for the local moment and the residual DOS comes from the itinerant bands. Initial doping into the latter will leave the large Mott-like gap intact and the gap bottom pinned at E_F, until the upper Hubbard band starts to get filled at strong overdoping. The existence of local moment can also be seen from the linear T dependence of magnetic susceptibility in the same $NaFe_{1-x}Co_xAs$ samples [15], which is consistent with the two dimensional Heisenberg model for local spins with AFM interaction [29].

Next we show that the local-itinerant coexistent model can give a consistent explanation for the three distinct phases. We start from the parent SDW state. The strongly asymmetric gap structure is energetically unfavorable for simple FS nesting. Moreover, neutron scattering finds that the SDW wave vector is always locked to $Q = (\pi, \pi)$ in the folded Brillouin zone notation, whereas in the FS nesting picture the SDW order is usually incommensurate and sensitive to detailed FS geometry. However, both anomalies seem to be natural from the local-itinerant coupling point of view. The (π, π) wave vector corresponds to the AFM ordering of the local moments as predicted by theory [30]. The large Hund's rule coupling between the local moments and itinerant electrons can stabilize this commensurate SDW order and lead to the large $2\Delta/k_BT_{SDW}$ ratio. The deviation of gap bottom from E_F and the particle-hole asymmetry are due to the asymmetric Γ and M pockets with respect to E_F. When they are forced to shift along the (π, π) direction by electron-hole scattering, they may intersect at an energy away from E_F and open a gap there, as illustrated in Fig. 5(c).

In the optimally doped regime, the SDW gap disappears, indicating the absence of long-range AFM ordering. However, short-range AFM correlations between the local moments do exist, as seen from the linear T dependence of magnetic susceptibility [15]. It has been proposed that the short-range AFM correlated local moments can support

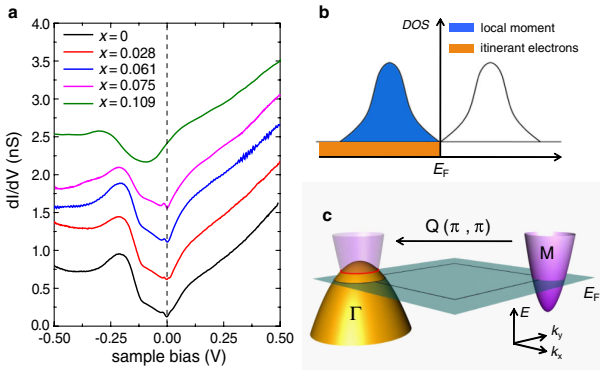

FIG. 5 (color online). (a) High energy dI/dV spectra of $NaFe_{1-x}Co_xAs$ taken at $T = 5$ K. The bottom of the V-shaped DOS suppression is pinned at E_F up to $x = 0.075$, but shifts to the left significantly at $x = 0.109$. (b) Schematic electronic structure of the local-itinerant coexistent model. (c) A cartoon shows the band crossing for electron-hole scattering with (π, π) wave vector in the folded Brillouin zone notation.

gapped spin waves, or massive magnons [9,10]. Because of the Hund's rule coupling, the magnons can be emitted or absorbed by itinerant electrons via spin exchange, which provides an effective attraction in a similar manner to the phonon-mediated BCS mechanism.

The pseudogaplike phase in the overdoped regime is more puzzling. The strong spatial variations indicate that it is a local phenomenon without long-range ordering. The localized character also rules out the simple band structure effect as a possible origin. The similarities between the pseudogaplike feature and the parent SDW gap in terms of gap size, shape, and T evolution suggest that it may originate from a similar mechanism, except for the lack of long-range AFM ordering in the overdoped regime. In fact it has been shown theoretically that the scattering between the local moments and itinerant electrons via the Hund's rule coupling may generate a pseudogap with characteristic peak-dip structure at E_F similar to the spectral features discovered here [31].

It is recently proposed that the preemptive nematic order could also give rise to a pseudogap in the fermionic spectral function due to the thermal magnetic fluctuation [32]. This pseudogap is expected to have similar features as the spectral gap in the magnetically order phase, which is consistent with our observation that the pseudogaplike feature is similar to the parent SDW gap. The T_{onset} of the pseudogaplike feature is also close to $T_S = 54$ K in parent NaFeAs when the nematic order sets in [32]. However, it is unclear at the moment if the nematic model can apply to the overdoped regime.

In summary, STM studies on $NaFe_{1-x}Co_xAs$ shed important new lights on the nature and relationship of various phases in the iron pnictides. The optimally doped sample has neither SDW nor pseudogaplike feature, suggesting that these two phases compete with the SC order, either for the itinerant FS sections or scattering channels with the local moments. On the other hand, the simultaneous disappearance of the SC and pseudogaplike features in the non-SC overdoped sample suggests that they are closely related. They both originate from the Hund's rule coupling between local moments and itinerant electrons, which may diminish in the strongly overdoped regime when the sinking of the hole pocket at the Γ point invalidates the inter pocket scattering process.

This work was supported by the National Natural Science Foundation of China and the Ministry of Science and Technology of China (grant No. 2009CB929400, 2010CB923003, and 2011CBA00101).

*yayuwang@tsinghua.edu.cn

[1] J. Zhao *et al.*, Nature Mater. **7**, 953 (2008).
[2] H. Luetkens *et al.*, Nature Mater. **8**, 305 (2009).
[3] I. I. Mazin, D. J. Singh, M. D. Johannes, and M. H. Du, Phys. Rev. Lett. **101**, 057003 (2008).
[4] A. V. Chubukov, D. V. Efremov, and I. Eremin, Phys. Rev. B **78**, 134512 (2008).
[5] F. Wang, H. Zhai, Y. Ran, A. Vishwanath, and D.-H. Lee, Phys. Rev. Lett. **102**, 047005 (2009).
[6] V. Cvetkovic and Z. Tesanovic, Europhys. Lett. **85**, 37002 (2009).
[7] Q. Si and E. Abrahams, Phys. Rev. Lett. **101**, 076401 (2008).
[8] K. Seo, B. A. Bernevig, and J. Hu, Phys. Rev. Lett. **101**, 206404 (2008).
[9] S.-P. Kou, T. Li, and Z.-Y. Weng, Europhys. Lett. **88**, 17010 (2009).
[10] Y.-Z. You, F. Yang, S.-P. Kou, and Z.-Y. Weng, Phys. Rev. B **84**, 054527 (2011).
[11] J. E. Hoffman, Rep. Prog. Phys. **74**, 124513 (2011).
[12] W. Z. Hu, G. Li, P. Zheng, G. F. Chen, J. L. Luo, and N. L. Wang, Phys. Rev. B **80**, 100507 (2009).
[13] F. Massee, Y. K. Huang, J. Kaas, E. van Heumen, S. de Jong, R. Huisman, H. Luigjes, J. B. Goedkoop, and M. S. Golden, Europhys. Lett. **92**, 57 012 (2010).
[14] Y. M. Xu *et al.*, Nature Commun. **2**, 392 (2011).
[15] A. F. Wang, X. G. Luo, Y. J. Yan, J. J. Ying, Z. J. Xiang, G. J. Ye, P. Cheng, Z. Y. Li, W. J. Hu, and X. H. Chen, Phys. Rev. B **85** 224521 (2012).
[16] See Supplemental Material at http://link.aps.org/supplemental/10.1103/PhysRevLett.109.037002 for more topographic images and dI/dV spectroscopy of the parent and Co-doped samples.
[17] T. Hänke, S. Sykora, R. Schlegel, D. Baumann, L. Harnagea, S. Wurmehl, M. Daghofer, B. Büchner, J. van den Brink, and C. Hess, Phys. Rev. Lett. **108**, 127001 (2012).
[18] H. Yang *et al.*, arXiv:1203.3123.
[19] S. Chi *et al.*, arXiv:1204.0273.
[20] G. F. Chen, W. Z. Hu, J. L. Luo, and N. L. Wang, Phys. Rev. Lett. **102**, 227004 (2009).
[21] S. Li, C. de la Cruz, Q. Huang, G. F. Chen, T.-L. Xia, J. L. Luo, N. L. Wang, and P. Dai, Phys. Rev. B **80**, 020504 (2009).
[22] Ch. Renner, B. Revaz, J.-Y. Genoud, K. Kadowaki, and Ø. Fischer, Phys. Rev. Lett. **80**, 149 (1998).
[23] K. McElroy, D.-H. Lee, J. E. Hoffman, K. M. Lang, J. Lee, E. W. Hudson, H. Eisaki, S. Uchida, and J. C. Davis, Phys. Rev. Lett. **94**, 197005 (2005).
[24] M. C. Boyer, W. D. Wise, K. Chatterjee, M. Yi, T. Kondo, T. Takeuchi, H. Ikuta, and E. W. Hudson, Nature Phys. **3**, 802 (2007).
[25] J. Wu, P. Phillips, and A. H. Castro Neto, Phys. Rev. Lett. **101**, 126401 (2008).
[26] L. de' Medici, S. Hassan, and M. Capone, J. Supercond. Novel Magnetism **22**, 535 (2009).
[27] A. Hackl and M. Vojta, New J. Phys. **11**, 055064 (2009).
[28] W.-G. Yin, C.-C. Lee, and W. Ku, Phys. Rev. Lett. **105**, 107004 (2010).
[29] G. M. Zhang, Y. H. Su, Z. Y. Lu, Z. Y. Weng, D. H. Lee, and T. Xiang, Europhys. Lett. **86**, 37006 (2009).
[30] T. Yildirim, Phys. Rev. Lett. **101**, 057010 (2008).
[31] A. Liebsch, Phys. Rev. B **84**, 180505 (2011).
[32] R. M. Fernandes, A. V. Chubukov, J. Knolle, I. Eremin, and J. Schmalian, Phys. Rev. B **85**, 024534 (2012).